Magnetism in the linear-chain antiferromagnet $RbCoCl_3 \cdot 2H_2O$ studied by dynamic susceptibility and electron-spin resonance

E. J. Nijhof, H. van der Vlist, J. A. Puértolas,* and G. J. Gerritsma
Department of Applied Physics, Twente University of Technology, NL-7500AE Enschede, The Netherlands
(Received 26 September 1985)

The magnetism in $RbCoCl_3 \cdot 2H_2O$ ($T_N = 2.97$ K) is studied by high-temperature dynamic susceptibility and low-temperature electron-spin resonance. In order to describe the experiments a Hamiltonian is derived that includes spin-orbit coupling, tetragonal and rhombic distortions, exchange in the mean-field approximation, and an external magnetic field. A simultaneous fit to three mutual perpendicular susceptibilities yields consistent values for the crystal-field parameters and an intrachain exchange constant of $J/k_B = -5.0$ K. The final Hamiltonian in the effective-spin $s = \frac{1}{2}$ formalism is more or less of the planar type. The zero-field electron-spin-resonance spectra are described in terms of magnon bound states, i.e., the elementary excitations of the proposed Hamiltonian. The frequency independence and the angular dependence of both microwave and external fields are explained by the model. The temperature variations of the absorption intensity and linewidth are qualitatively discussed using simplified models.

I. INTRODUCTION

The hydrated compounds $AMCl_3 \cdot 2H_2O$, with $A = Cs$, Rb, or $(CH)_3NH$ and $M = Co$ or Fe, are prototypes of chainlike metamagnetic systems,[1] and show a great variety of canted (anti-) ferromagnetic structures.[2-5] They are characterized by weakly coupled chains which themselves possess strong (Ising-like) intrachain exchange interactions. Apart from many interesting (field-induced) phase-transition properties, this quasi-one-dimensional behavior has made these compounds the subject of a great number of experimental studies.[2-12] The present system, $RbCoCl_3 \cdot 2H_2O$ (RCC), shares many properties with the other family members. It distinguishes itself, however, by a different crystal structure (monoclinic),[13] a relatively low field of the metamagnetic phase transition (70 Oe),[14] and a plane of magnetic ordering which does not coincide with a typical plane of the crystallographic structure.[5,12]

The present interest in RCC stems from the following considerations. From a study of the low-temperature susceptibility and specific heat, McElearney and Merchant[13] proposed that RCC might be an example of a Dzyaloshinsky-Moriya (DM) linear-chain magnet, i.e., antisymmetric exchange is the dominating intrachain interaction. Neutron-diffraction results[5] showed, however, that in the ordered state the canting of the sublattices was not compatible with a pure DM interaction. To elucidate this apparent contradiction we have studied the magnetic interactions from a microscopic point of view. We derived a spin Hamiltonian including the exchange interactions, thereby taking into account the canting of the local surroundings of the magnetic ions. Experimental information was gained from high-temperature susceptibilities in such a way that the problem of interference of pure one-dimensional (1D) behavior and 3D ordering phenomena was avoided. This latter complicated metamagnetic behavior of RCC has recently been reconsidered by Flokstra *et al.*[15]

In connection with the antisymmetric exchange, it makes sense to inquire into the nature of the elementary excitations at temperatures just above or in the ordered regime. By virtue of its multicomponent character, the DM model can give rise to linear excitations (magnon-bound states) as well as to nonlinear excitations (solitons). If, on the other hand, an Ising-like interaction is present, spin clusters are the dominating linear excitations. We report here on the excitations in RCC which are characterized by strong microwave absorption in zero external field, and an angular dependence pointing to strong anisotropic behavior.

To make this paper self-contained, we shall now sum-

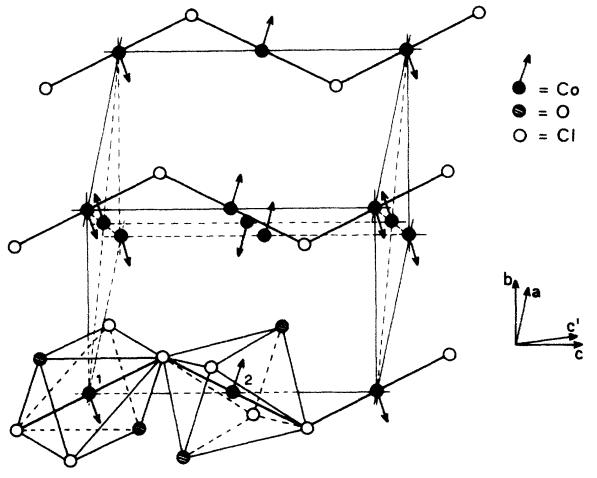

FIG. 1. Monoclinic unit cell of $RbCoCl_3 \cdot 2H_2O$. Cell constants are $a = 15.714$ Å, $b = 5.619$ Å, $c = 8.743$ Å, and $\beta = 118.37°$ (Ref. 13). (Rb and H atoms are not indicated.) Arrows denote the magnetic moments in the ordered phase and are located in b-c' planes. The c' axis makes an angle of 22° in the a-c plane with the c axis (Ref. 17). Notation of (1) and (2) at the octahedra is explained in the text.

marize some crystallographic and magnetic properties of RCC.[16] The crystal structure is face-centered monoclinic (space group $C2/c$, Fig. 1).[5,13] The Co ions are octahedrally surrounded by four chlorine atoms and two H_2O molecules. The *trans*-$[CoCl_4(H_2O)_2]$ octahedra form chains along the c direction. In zero external field RCC orders antiferromagnetically at $T_N=2.97$ K. Vermeulen *et al.*[5] determined the magnetic space group C_p2'/c from NMR and neutron-diffraction data. The magnetic moments are located in b-c' planes, where c' is at an angle of $22°\pm1°$ with the c axis.[17] The canting of the magnetic moments amounts to $17°\pm5°$ with respect to the b axis. The components along the c' axis are ferromagnetically aligned. The ordering between the chains is ferromagnetic in the b-c plane, while the relative orientation of adjacent b-c planes is antiparallel.[5]

The paper is arranged as follows. In the next section some experimental details are given. In Sec. III the susceptibility data are discussed, and in Sec. IV we present the resulting spin Hamiltonian. The ESR measurements, together with a semiquantitative interpretation, are given in Sec. V. Finally, the paper ends with a summary and some conclusions in Sec. VI.

II. EXPERIMENTAL DETAILS

Single crystals of $RbCoCl_3\cdot2H_2O$ were grown by slowly evaporating an aqueous solution of RbCl and $CoCl_2\cdot6H_2O$ (molar ratio 1:4.44) at a temperature of about 30 °C. The crystals grew as prisms elongated along the [001] direction and with average dimensions of $2\times2\times5$ mm^3. The crystal structure was verified by x-ray diffraction.

Below 100 K dynamic susceptibilities were measured with an ac susceptometer[18] using a mutual-inductance technique. Typical values for the frequency and the amplitude of the alternating magnetic field were 330 Hz and 1 Oe, respectively. The system was calibrated using the known susceptibility of $Mn(NH_4)_2(SO_4)_2\cdot6H_2O$. The sensitivity amounted to 10^{-6} emu. Temperature control was accomplished by feedback-controlled heating of He gas in the sample space, which was in direct contact with a liquid-He bath. Temperatures were measured with a calibrated carbon-glass resistor. The susceptibility data were taken in various crystallographic directions by the use of appropriate wedges. At room temperature the static susceptibility was measured with a superconducting quantum-interference device (SQUID) magnetometer with an open-ended horizontal access.[19] Angular variation was obtained by repositioning the crystal relative to the fixed direction of the static magnetic field.

The ESR measurements were carried out on a conventional X-band microwave spectrometer, operating at a fixed frequency near 9.5 GHz, and fitted for direct recording of the absorption signal. The sample was mounted on a rotation table in the center of a rectangular resonant cavity, operating in the TE_{102} mode. The magnetic field was applied along the cavity by a 3-T superconducting magnet. In addition, a number of measurements were performed in a parallel-field configuration, in which case the sample was mounted on a narrow wall of the cavity. Temperature control below 4.2 K was effected by reducing the pressure above the liquid-He bath. Stabilization within 0.01 K was achieved by using a manostat. Above 4.2 K the sample space of the cryostat was filled with He gas to cool the sample by means of conduction. Temperature stabilization within 0.03 K was obtained by feedback-controlled heating. A carbon-glass resistor was used to measure the temperature.

III. SUSCEPTIBILITIES

In this section a general model for the high-temperature susceptibilities in an exchange-coupled system with a canted structure is derived. From a fit to experimental data we can deduce crystal-field parameters which serve as the input for a spin Hamiltonian for $RbCoCl_3\cdot2H_2O$.

A. Theory

The ligand field of the Co^{2+} ion in RCC is determined by the trans-octahedral surroundings (cf. Fig. 1). The directions of the Co—O and Co—Cl bonds in the case of RCC are almost orthogonal. So we introduce a set (ξ,η,ζ) of local coordinate axes along these bonds, i.e., ζ in the Co-O direction, ξ in the Co-Cl chain direction, and η along the remaining Co—Cl bond (Fig. 2). Note that these axes are different for two neighboring Co^{2+} ions in the chain. Justification for choosing the principal axes of the crystal field in this way will be given in the discussion below. Details about Co^{2+} in such a ligand field are given by Oguchi[20] and Narath[21] in their treatments of $CoCl_2\cdot2H_2O$.

The general state of Co^{2+} ($S=\frac{3}{2}$) in a cubic crystal field is an orbital triplet ($^4T_1$). The main perturbation arises from the spin-orbit coupling and noncubic distortions of the crystal field, represented by the Hamiltonian

$$\mathcal{H}=-\tfrac{3}{2}k\lambda\boldsymbol{l}\cdot\mathbf{S}-\Delta[(l^\xi)^2-\tfrac{2}{3}]-\Gamma[(l^\eta)^2-(l^\xi)^2]\ . \quad (1)$$

Within the $^4T_1$ triplet the angular momentum is defined

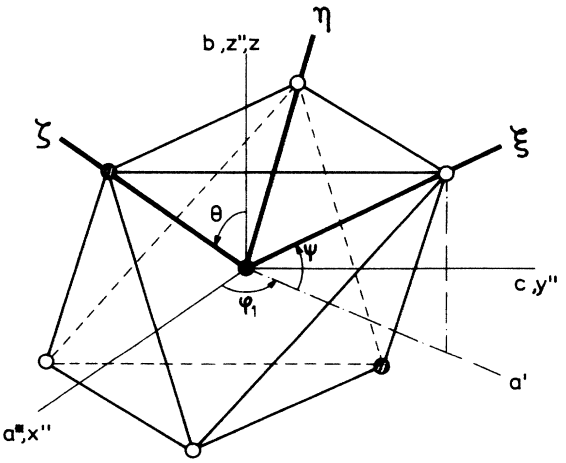

FIG. 2. Definition of the local coordinate system type (1). Eulerian angles are specified by $\phi_1=61.4°$ (rotation in the a-c plane), $\theta=44.5°$ (rotation around a'), and $\psi=38.9°$ (rotation around ζ). For type (2), $\phi_2=\phi_1+\pi$, and the θ and ψ are rotated in the same direction as (1).

by $\mathbf{L}=-\frac{3}{2}\boldsymbol{l}$ with $l=1$. The spin-orbit-coupling constant is λ, while k is a correction factor due to the mixing with higher orbital levels and effects of covalent binding.[22] The last two terms of Eq. (1) denote the effects of tetragonal (Δ) and rhombic (Γ) distortion, respectively. The perturbation $\mathscr{H}$ splits the 3×4 degenerate $^4T_1$ level in six Kramers doublets. For the sake of convenience new crystal-field parameters are introduced in the numerical calculation,[21]

$$\Delta=\tfrac{1}{2}D(3+\kappa),\quad \Gamma=\tfrac{1}{2}D(1-\kappa)\ , \tag{2}$$

where κ is a measure for the antisymmetry, $-1\leqq\kappa\leqq1$.

Rewriting Eq. (1) yields

$$\mathscr{H}=-\tfrac{3}{2}\lambda'\boldsymbol{l}\cdot\mathbf{S}+D[(l^{\xi})^2+\kappa(l^{\eta})^2-(l^{\zeta})^2]-\tfrac{2}{3}D\kappa\ , \tag{3}$$

where $\lambda'=k\lambda$. The matrix elements of $\mathscr{H}$ are calculated in the $|\,l,l^{\zeta};S,S^{\zeta}\rangle$ representation of the $^4T_1$ state, yielding two degenerate sets which we denote by $|+\rangle$ and $|-\rangle$. The matrix $\underline{M}=\langle\pm|\mathscr{H}|\pm\rangle$ is diagonalized by a unitary transformation $\underline{U}$, according to

$$E_{0,i}=\langle i\,|\,\underline{U}^{-1}\underline{M}\,\underline{U}\,|\,i\rangle\ , \tag{4}$$

where $|\,i\rangle$ ($i=1,\ldots,6$) denotes the eigenstate of $\underline{M}$ with energy $E_{0,i}$. The remaining degeneracy of the Kramers doublets is lifted by the Zeeman interaction

$$\mathscr{H}_Z=-\tfrac{3}{2}k\mu_B\mathbf{H}\cdot\boldsymbol{l}+2\mu_B(\mathbf{H}+\mathbf{H}_e)\cdot\mathbf{S}\ , \tag{5}$$

where $\mathbf{H}$ is the external magnetic field and $\mathbf{H}_e$ represents the exchange field in the mean-field approximation. Up to second order in $\mathscr{H}_Z$ the energies are modified to

$$E^{\alpha}_{\pm,i}=E_{0,i}\pm\langle i\,|\,\mathscr{H}^{\alpha}_Z\,|\,i\rangle+\sum_{j\neq i}\frac{|\,\langle i\,|\,\mathscr{H}^{\alpha}_Z\,|\,j\rangle\,|^2}{E_{0,i}-E_{0,j}}\ , \tag{6}$$

with $\alpha=\xi,\eta,\zeta$ and $i,j=1,\ldots,6$. The susceptibilities can now be calculated from the energies $E^{\alpha}_{\pm,i}$. Before doing so, however, we first have to specify the exchange field $\mathbf{H}_e$.

In the full spin notation ($S=\frac{3}{2}$) the exchange between two neighboring Co spins is assumed to be isotropic, i.e.,

$$\mathscr{H}_e=-2J\mathbf{S}_1\cdot\mathbf{S}_2\ , \tag{7}$$

where the components of $\mathbf{S}_1$ and $\mathbf{S}_2$ are expressed on the same, crystallographic, set of axes. For the latter we use the interchangeable notations x'',y'',z'' or a^*,c,b, where a^* denotes the normal of the b-c plane. To calculate the susceptibility, and anticipating a transformation to an effective spin $s=\frac{1}{2}$ notation, it is convenient to express H_e in terms of local crystal-field axes.[6,23] The octahedra are canted with respect to each other in the c (or chain) direction. We therefore distinguish two sublattices, subscripted (1) and (2), with their own local axes [cf. Fig. 1; (1) is depicted in Fig. 2]. The local axes are parametrized by the Eulerian angles $\phi_{1,2}$, θ, and ψ, where $\phi_2=\phi_1+\pi$. For details on the transformations we refer to the Appendix. The result for the exchange of spin (1) in the mean-field notation reads

$$\mathscr{H}_e=2\mu_B\mathbf{H}_{e,1}\cdot\mathbf{S}_1\ , \tag{8}$$

with

$$\mathbf{H}_{e,1}=\begin{bmatrix}H^{\xi}_{e,1}\\H^{\eta}_{e,1}\\H^{\zeta}_{e,1}\end{bmatrix}=-\frac{J}{\mu_B}\underline{E}\begin{bmatrix}\langle S^{\xi}_2\rangle\\\langle S^{\eta}_2\rangle\\\langle S^{\zeta}_2\rangle\end{bmatrix}\ , \tag{9}$$

and the matrix $\underline{E}$ is defined in the Appendix. The angular brackets denote the statistical average of the operator. It should be kept in mind that the components of $\mathbf{S}_2$ are referred to a set of local axes in octahedron type (2).

The susceptibility in the direction of a principal axis α ($\alpha=\xi,\eta,\zeta$) for ion type (1) is defined by

$$\chi^{\alpha}_1=\frac{N}{\beta H^{\alpha}_1}\frac{1}{Z^{\alpha}}\frac{\partial Z^{\alpha}}{\partial H^{\alpha}_1}\ , \tag{10}$$

where $Z^{\alpha}=\sum_{\pm i}\exp(-\beta E^{\alpha}_{\pm,i})$ denotes the partition function, $\beta=1/k_BT$, and N is Avogadro's number. The energies $E^{\alpha}_{\pm,i}$ are calculated from Eq. (6) and yield

$$E^{\alpha}_{\pm,i}=E_{0,i}\pm[-\tfrac{3}{2}k\mu_BH^{\alpha}_1\langle i\,|\,l^{\alpha}\,|\,i\rangle+2\mu_B(H^{\alpha}_1+H^{\alpha}_e)\langle i\,|\,S^{\alpha}\,|\,i\rangle]+\sum_{j\neq i}\frac{[-\frac{3}{2}k\mu_BH^{\alpha}_1\langle i\,|\,l^{\alpha}\,|\,j\rangle+2\mu_B(H^{\alpha}_1+H^{\alpha}_e)\langle i\,|\,S^{\alpha}\,|\,j\rangle]^2}{E_{0,i}-E_{0,j}}\ . \tag{11}$$

We restrict ourselves to a high-temperature approximation, i.e., we assume that the perturbation energy due to $\mathscr{H}_e$ is small compared to k_BT. In this case the expression for χ^{α}_i is restricted to

$$\chi^{\alpha}_1=P^{\alpha}_1+Q^{\alpha}_1\frac{H^{\alpha}_{e,1}}{H^{\alpha}_1}\ , \tag{12}$$

with

$$P^{\alpha}_1=\frac{2N}{Z^{\alpha}}\sum_i\exp(-\beta E_{0,i})\left[\beta A_{ii}-2\sum_{j\neq i}\frac{A_{ij}}{E_{0,i}-E_{0,j}}\right]\ , \tag{13a}$$

$$Q^{\alpha}_1=\frac{4N}{Z^{\alpha}}\sum_i\exp(-\beta E_{0,i})\left[\beta B_{ii}-2\sum_{j\neq i}\frac{B_{ij}}{E_{0,i}-E_{0,j}}\right]\ , \tag{13b}$$

and

$$A_{ij}=(-\tfrac{3}{2}k\mu_B\langle i\,|\,l^{\alpha}\,|\,j\rangle+2\mu_B\langle i\,|\,S^{\alpha}\,|\,j\rangle)^2\ , \tag{14a}$$

$$B_{ij}=-3k\mu_B^2\langle i\,|\,l^{\alpha}\,|\,j\rangle\langle i\,|\,S^{\alpha}\,|\,j\rangle+4\mu_B^2\langle i\,|\,S^{\alpha}\,|\,j\rangle^2\ . \tag{14b}$$

Upon replacing $H^{\alpha}_{e,1}$ in Eq. (12) with $H^{\alpha}_{e,2}$, the susceptibilities of sublattice (2) may be derived in a similar way. It should be noted that H^{α}_1 generates three spin components

at sublattice (2). In order to solve Eq. (12) we make the approximation

$$\chi_2^\alpha = N g^\alpha \mu_B \langle S_2^\alpha \rangle / H_2^\alpha \ , \tag{15}$$

where g^α are the spectroscopic splitting factors of the lowest Kramers doublet $|1^\pm\rangle$. These factors are defined by

$$g^\alpha = 2\langle 1^\pm | -\tfrac{3}{2} k l^\alpha + 2S^\alpha | 1^\mp \rangle \quad (\alpha = \xi, \eta) \ ,$$
$$g^\zeta = 2\langle 1^\pm | -\tfrac{3}{2} k l^\zeta + 2S^\zeta | 1^\pm \rangle \ . \tag{16}$$

The final step is to drop the indices (1) and (2) of the χ's, which is accomplished by expressing H_1^α in H_2^α using the transformations $\underline{R}_1$ and $\underline{R}_2$ as defined in the Appendix.

The susceptibilities are now the solutions of

$$\underline{C}\chi = \mathbf{P} \ , \tag{17}$$

where

$$\underline{C} = \begin{bmatrix} 1-\alpha^2 F^\xi/g^\xi & -\nu^2 F^\xi/g^\eta & -\rho^2 F^\xi/g^\zeta \\ -\nu^2 F^\eta/g^\xi & 1-\beta^2 F^\eta/g^\eta & -\sigma^2 F^\eta/g^\zeta \\ -\rho^2 F^\zeta/g^\xi & -\sigma^2 F^\zeta/g^\eta & 1-\gamma^2 F^\zeta/g^\zeta \end{bmatrix} , \tag{18}$$

$$F^\alpha = -2JQ^\alpha/N\mu_B^2 \ , \tag{19}$$

and the components of vector $\mathbf{P}$ are defined in Eq. (13a). The constants $\alpha,\beta,\gamma,\nu,\rho,\sigma$ are defined in the Appendix (matrix $\underline{E}$). It is obvious from Eq. (17) that a calculation starting from ion type (2) will give the same result. When a magnetic field is applied in an arbitrary direction, the measured susceptibility will be a linear combination of the χ^α. The transformation is straightforward when use is made of the matrices $\underline{R}_j$ [Eq. (A2)].

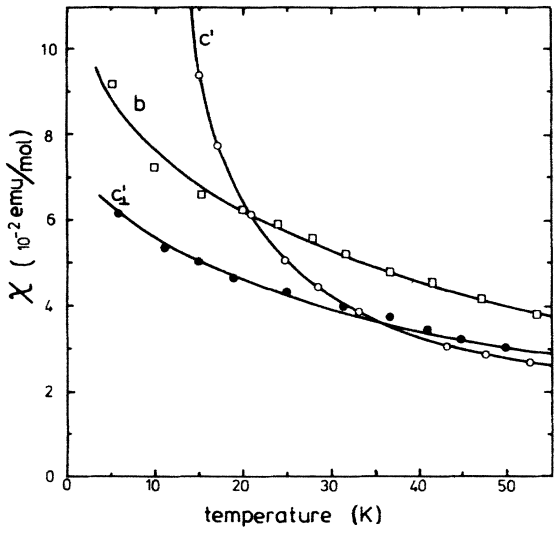

FIG. 3. Low-temperature ac susceptibility at zero field of $RbCoCl_3 \cdot 2H_2O$, taken along the b (□), c' (○), and c'_1 (●) axes. Solid lines are guides to the eye. The steep rise of c' data is due to increasing ferromagnetic order along the c' axis.

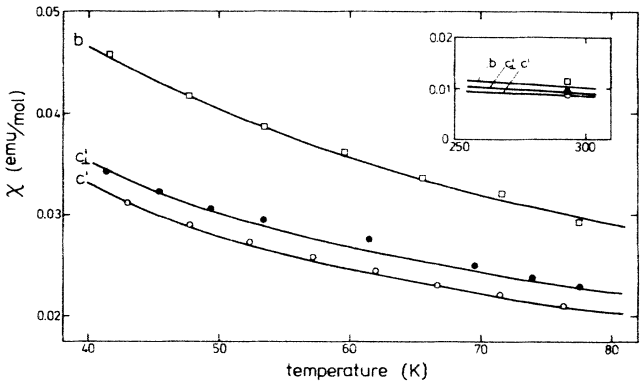

FIG. 4. High-temperature ac susceptibility at zero field of $RbCoCl_3 \cdot 2H_2O$, taken along b (□), c' (○), and c'_1 (●) axes. The inset shows static susceptibilities at zero field at room temperature. Solid lines are the fits to the data according to Sec. III B, in which the fitting parameters are discussed.

B. Results and discussion

Zero-field ac susceptibilities in the b, c' and c'_1 directions have been measured with the mutual-inductance method in the temperature region of 4.2 to 80 K (Figs. 3 and 4). Additional measurements, using the SQUID magnetometer, were performed at room temperature for χ along the b direction, as well as for several directions in the a-c plane (Fig. 5). The susceptibility along the b axis is, at high temperatures ($T > 40$ K), larger than that in the a-c plane, indicating that the b axis is the symmetry axis with the largest g factor. From the rotation diagram of Fig. 5 we deduce a maximum of χ close to the a^* axis and 180° periodicity. The above-mentioned facts indicate a behavior similar to that in related metamagnetic systems.[8,21,24] The low-temperature susceptibilities (Fig. 3) agree with the experimental results of McElearney and Merchant[12] in a qualitative way. The steep rise of $\chi^{c'}$ below 40 K is clearly seen, while the crossing of $\chi^{c'_1}$ and χ^b and $\chi^{c'}$ is more explicitly demonstrated than in Ref.

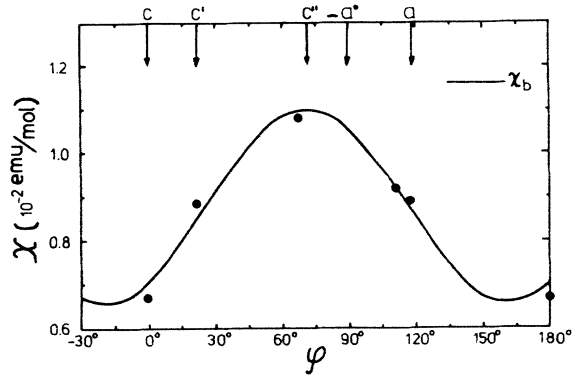

FIG. 5. Angular dependence of susceptibility of $RbCoCl_3 \cdot 2H_2O$ in the a-c plane at room temperature. Solid circles denote experimental data. Solid line is the fit according to Eq. (22). ϕ is the angle between applied magnetic field and the crystallographic c axis ($\phi = \Phi - 61.4°$). Arrows denote several important crystallographic directions; c'' is the calculated preferred direction of the moment (cf. Fig. 6).

12. It illustrates the important role of the relatively small ferromagnetic component, as is also known from other metamagnets.[8,25] We shall return to this point later.

A numerical procedure was set up to fit the experimental data to calculated susceptibilities, where the latter were obtained by transforming solutions of Eq. (17) to the relevant directions. In order to limit the number of fitting parameters we used well-established values for the spin-orbit interaction, $\lambda=-180$ cm^{-1},[20,26] and the orbital reduction factor, $k=0.9$.[22] The Eulerian angles as defined in Eq. (A2) (cf. Fig. 2) are derived from the atomic positions,[13] and amount to $\phi=61.4°$, $\theta=44.5°$, and $\psi=38.9°$. The distortion parameters D and κ, as well as the exchange constant J, are considered to be free. Due to the form of Eq. (17) the three susceptibilities had to be fitted simultaneously. Good fits, including the room-temperature data, were obtained for $T>40$ K, and the results are given by the solid lines in Fig. 4. We find

$$\begin{aligned} &D=320\pm5 \text{ cm}^{-1}, \\ &\kappa=0.46\pm0.05, \\ &J/k_B=-5.0\pm0.5 \text{ K}. \end{aligned} \tag{20}$$

The results for D and κ, together with λ and k, lead to a separation of the ground-state Kramers doublet and the first-excited state of 260 cm^{-1} [energies from Eq. (4)]. This value can be considered reasonable. It equals that in $CoCl_2\cdot2H_2O$ as reported by Oguchi,[20] and considering the ligand positions for both systems this correspondence is justified. The value of κ, however, points to a substantial asymmetry in the ξ-η plane, which is not *a priori* obvious in view of the geometrical symmetry of the Cl^- positions.[13] The parameter J will be discussed in the next section. In the course of the fitting procedure, the spectroscopic splitting factors, Eq. (16), are evaluated, and yield

$$g^{\xi}=3.4\pm0.3,\quad g^{\eta}=2.7\pm0.3,\quad g^{\zeta}=6.2\pm0.6. \tag{21}$$

They reflect the asymmetry in the ξ-η plane and confirm the strong tetragonal distortion along the ζ direction. The sum of these principal g factors equals 12 ± 1, which is, within the experimental errors, equal to 13, the theoretical value of a Co^{2+} ion in an octahedral environment.[26]

Attempts to extend the fits below 40 K failed because of two reasons. Firstly, the model we used was a high-temperature approximation. At the onset of increasing correlations in the chains, the mean-field approach, in particular, will no longer be valid. Secondly, a more severe problem arises from the increasing ferromagnetic component along the c' axis. Since the parallel susceptibility of a ferromagnet diverges, it eclipses in the present case all antiferromagnetic contributions in the c' direction (Fig. 3). This ferromagnetic susceptibility was studied by McElearney and Merchant,[12] and has recently been reconsidered in detail by Flokstra *et al.*[15] Furthermore, there will also be ferromagnetic disturbances in the b and $c'_\perp$ directions, including effects due to small misalignments during the measurements.

Finally, we draw attention to the difference between the present approach and the results of a Dzyaloshinsky-Moriya (DM) model as used in Ref. 12. For this purpose an approximation of Eq. (12) is worked out in which only the lowest Kramers doublet is taken into account, and where rhombic symmetry around the ζ axis is assumed ($\kappa=1$). The result, after transformation to crystallographic axes, reads[27]

$$\chi^{a\text{-}c}=\frac{\mu_B^2N}{4k_B}\left[\frac{(g^{\perp})^2}{T-(g_s^{\perp}/g_s^{\parallel})\Theta_N}\sin^2\Phi + \frac{\frac{1}{2}[(g^{\perp})^2+(g^{\parallel})^2](T-\Theta_0)}{(T+\Theta_N)(T-\Theta_N)}\cos^2\Phi\right], \tag{22}$$

$$\chi^{b}=\frac{\mu_B^2N}{4k_B}\frac{\frac{1}{2}[(g^{\perp})^2+(g^{\parallel})^2](T-\Theta_0)}{(T+\Theta_N)(T-\Theta_N)}, \tag{23}$$

with

$$\Theta_0=-\frac{g_s^{\parallel}g_s^{\perp}g^{\parallel}g^{\perp}}{2[(g^{\parallel})^2+(g^{\perp})^2]}J/k_B, \tag{24}$$

$$\Theta_N=\Theta_0\left[1-\frac{(g^{\parallel}+g^{\perp})^2}{2g^{\parallel}g^{\perp}}\right].$$

Here, Φ is the angle between the applied magnetic field and the projection of the ζ axis in the a-c plane. In the transformation $\underline{R}_j$ [Eq. (A2), $j=1,2$], we used $\theta=45°$ and, by virtue of symmetry, $\psi=0$. The notation for the g factors is evident, and the spin-only g factor g_s is defined in the next section. Equations (22) and (23) are, in fact, extensions of Moriya's results.[28] A fit to the experimental results using Eqs. (22) and (23) gives $D=231$ cm^{-1}, $J/k_B=-4.9$ K, $g^{\parallel}=6.0$, and $g^{\perp}=3.2$. In each direction b, c', and $c'_\perp$, a Van Vleck contribution was added as a variable parameter. The fits are as accurate as the previous ones (cf. Fig. 4). Apart from a different D value, which has to be attributed to the ligand symmetry, exchange constant and g values agree nicely in both models. In addition, Eq. (22) is used to fit the data in Fig. 5 (solid curve). No special significance of the c' axis at high temperatures is deduced from this figure. McElearney and Merchant[12] derived the second term on the right-hand side of Eq. (22) from the DM Hamiltonian, thereby prematurely assuming antisymmetric exchange. The conclusion must be, however, that, in the present case, antisymmetry, and hence canting of the sublattices, is brought about by the canting of the principle axes of the ligand fields alone. Furthermore, due to this canting a second contribution in $\chi^{a\text{-}c}$ arises which cannot be found from the DM model.

Concluding this section, we state that good fits for the high-temperature susceptibility were obtained, from which we derived reasonable values for the crystal-field and exchange parameters.

IV. SPIN-$\frac{1}{2}$ HAMILTONIAN

The low-temperature magnetic properties of $RbCoCl_3 \cdot 2H_2O$ can be described in terms of the ground-state Kramers doublet. This makes sense in view of the distance of 260 cm^{-1} between the latter and the first-excited state. In case the exchange Hamiltonian is written on the principal axes of the g tensor, the transformation to $s=\frac{1}{2}$ is accomplished by $S^\lambda=\frac{1}{2}g_s^\lambda s^\lambda$ ($\lambda=\xi,\eta,\zeta$). The result then reads [cf. Eq. (A3)]

$$\mathcal{H}_e=-\tfrac{1}{2}J\sum_{\langle l,m\rangle}[\alpha(g_s^\xi)^2 s_l^\xi s_m^\xi+\beta(g_s^\eta)^2 s_l^\eta s_m^\eta+\gamma(g_s^\zeta)^2 s_l^\zeta s_m^\zeta$$
$$+\nu g_s^\xi g_s^\eta(s_l^\xi s_m^\eta+s_l^\eta s_m^\xi)+\rho g_s^\xi g_s^\zeta(s_l^\xi s_m^\zeta+s_l^\zeta s_m^\xi)+\sigma g_s^\eta g_s^\zeta(s_l^\eta s_m^\zeta+s_l^\zeta s_m^\eta)]\,, \tag{25}$$

where l and m run over the sublattices (1) and (2), respectively, which each have their own set of principle axes. In the first term, summation over pairs is understood. The constants α, β, etc. are defined in Eq. (A5). The spin-only g factors are defined analogously to Eq. (16); however, here the wave functions are sandwiched between S^λ only. The numerical values are

$$g_s^\xi=2.7\pm0.3,\quad g_s^\eta=2.3\pm0.3,\quad g_s^\zeta=4.6\pm0.4\,. \tag{26}$$

Diagonalization of Eq. (25) is now straightforward. We then attain

$$\mathcal{H}_e=-2J_0\sum_{\langle l,m\rangle}(-ps_l^{\xi'}s_m^{\xi'}-qs_l^{\eta'}s_m^{\eta'}+s_l^{\zeta'}s_m^{\zeta'})\,, \tag{27}$$

with

$$J_0/k_B=-14.6\text{ K},\quad p=0.56,\quad q=0.98\,. \tag{28}$$

The primed coordinate system is the set of eigenvectors of the diagonalizing transformation, where the ζ' axis is taken in the direction of the largest anisotropy. Hence the ζ' axis is considered the equilibrium axis for the spins, as far as intrachain exchange is concerned. As to Eq. (27), we make the striking observation that the exchange interaction has an XY character rather than an Ising one. This is due to the severe canting of the local surroundings of the Co^{2+} ions and, in particular, the fact that $\theta=44.6°$ [cf. Eq. (A2)] does play a decisive role. The ζ' axis coincides with the crystallographic b axis by a very good approximation. The ξ' and η' directions are obtained from a rotation in the a-c plane, where the ξ' axis makes an angle $\phi'=39.2°$ with a^* (Fig. 6). Thus a formal back transformation is performed from the distinct local coordinate systems l and m to a single set of axes xyz, where z coincides with z''. Note that this formal step is necessary to remove the minus signs in Eq. (27), establishing the antiferromagnetic character of the system. The Hamiltonian is finally given by

$$\mathcal{H}_0=\mathcal{H}_e+\mathcal{H}_{(1)}+\mathcal{H}_Z+\mathcal{H}_{(2)}\,, \tag{29}$$

with

$$\mathcal{H}_e=-2J_0\sum_l(ps_l^x s_{l+1}^x+qs_l^y s_{l+1}^y+s_l^z s_{l+1}^z)\,, \tag{30}$$

$$\mathcal{H}_{(1)}=-\mu_B g^{zz}(H_{i,1}^z+H_d^z)\sum_l(-1)^l s_l^z\,, \tag{31}$$

$$\mathcal{H}_Z=-\mu_B\sum_l \mathbf{s}_l^T\underline{G}_l\mathbf{H}\,. \tag{32}$$

The interchain exchange field $H_{i,1}$ between chains in a b-c plane is defined analogously to Eq. (9), where only the Ising term is retained. In addition, we introduced an (Ising) dipolar field H_d^z. This field is found from evaluating the dipolar interactions over a limited number of shells. Full account is taken, however, of the direction of the moments. The result amounts to $H_d^z\approx1.5$ kOe at $T=0$. The g^λ factors along the principle axes were calculated in the preceding section [Eq. (21)]. Transformation of this diagonal tensor to the xyz axes is accomplished by the use of R_j [Eq. (A2), $j=1,2$] with the substitution of $\phi\to\phi-\phi'$ (cf. Fig. 6). This yields

$$\underline{G}_l=\begin{bmatrix}3.2 & -0.4 & 0.8(-1)^l\\ -0.4 & 4.5 & 1.4(-1)^l\\ -0.8(-1)^l & 1.4(-1)^l & 4.6\end{bmatrix}\,, \tag{33}$$

where the $(-1)^l$ accounts for the difference in canting of the spins on the up and down sublattices. From Eq. (33) we see that g^{zz} in Eq. (31) amounts to 4.6. Finally, $\mathcal{H}_{(2)}$ represents the resulting interplane interaction. This energy is very small, as may be inferred from the metamagnetic transition at 70 Oe, and zero temperature.[14,15]

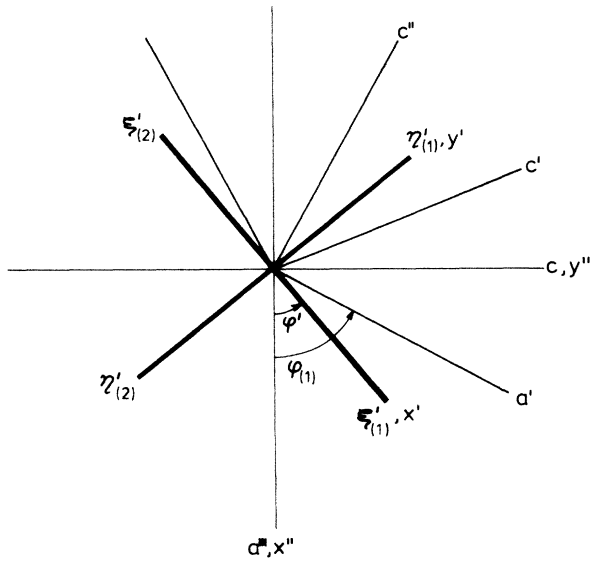

FIG. 6. Directions of coordinate axes in the a^*-c plane. Notations are explained in the text. Positive axes of sublattice (2) ($\xi'_{(2)}$, $\eta'_{(2)}$) are rotated over 180° with respect to those of sublattice (1), and $\phi'=39.2°$.

From the tensor $\underline{G}_l$ presented above, we can calculate the length and direction of the magnetic moments. Assuming $s^z = +\frac{1}{2}, -\frac{1}{2}$ for ions type (1) and (2), respectively, the resulting moments are

$$\mu_{1\,(2)} = -\mu_B \underline{G}_{1\,(2)} \mathbf{s}_{1\,(2)}$$
$$= [-0.4, 0.7, -(+)2.3]\mu_B \ , \qquad (34)$$

which gives a component $2.3\mu_B$ along the z axis, and a deviation of 19° from that axis. Both values, and also the length of the moments $\mu = 2.4\mu_B$, are in excellent agreement with the neutron-diffraction results of Vermeulen *et al.*[5] The calculated direction of $\mu^{a\text{-}c}$ makes an angle of 70° with the c axis (c'' axis, cf. Fig. 6), which is seen to correspond with the measured direction of $\chi^{a\text{-}c}_{\max}$ at high temperatures (Fig. 5). This justifies, in retrospect, the choice of the set of axes for the ligand fields. It is also clear by now that canting of the moments, and hence the rise of a ferromagnetic component, is primarily due to the canting of subsequent crystal-field axes. The question that remains is why the preferred direction in the a-c plane turns to the c' axis in the ordered state? In the above model it can be accounted for by the rise of a spin component in the x direction. In view of the fact that the c' axis is almost perpendicular to the a axis, the rotation of $\mu^{a\text{-}c}$ at the onset of 3D ordering is likely due to the monoclinic structure of RCC and the small, but complicated interplane interactions, which give rise to the necessary anisotropy.

We finally comment on the intrachain exchange. The value $J_0/k_B = -14.6$ K for the exchange constant is close to the result of McElearney and Merchant,[12] $J/k_B = +12$ K. Note that in the latter case this ferromagnetic J value is obtained from a fit of a 1D Ising model to the low-temperature $\chi^{c'}$. A similar kind of analysis was recently performed by Flokstra *et al.*,[15] yielding $J/k_B = +12.6$ K. From the analysis given above it is clear that canting of the magnetic moment can be fully explained by the crystallographic structure, together with the single-ion anisotropies. Hence we can disregard any antisymmetric exchange. Off-diagonal exchange terms arise when evaluating the Hamiltonian on different local axes for the sublattices [cf. Eq. (25)], the symmetry or antisymmetry depending on the choice of Eulerian angles. At this point the main difference between the present analysis and that of McElearney and Merchant[12] becomes apparent. In the latter case the antisymmetry was assumed to be present in the crystallographic coordinate system, which does not seem to be the case for the present compound. The effect of the canting of the octahedra is better expressed in symmetric non-Ising terms of the exchange Hamiltonian.

V. ESR IN $RbCoCl_3 \cdot 2H_2O$

A. Experimental results

Microwave measurements at frequencies near 9.5 GHz were performed on single crystals of $RbCoCl_3 \cdot 2H_2O$.[16] Spectra were recorded in several crystal planes. Upon rotating the crystal, the relative orientations of both the microwave and the static fields were changed with respect to the crystal.

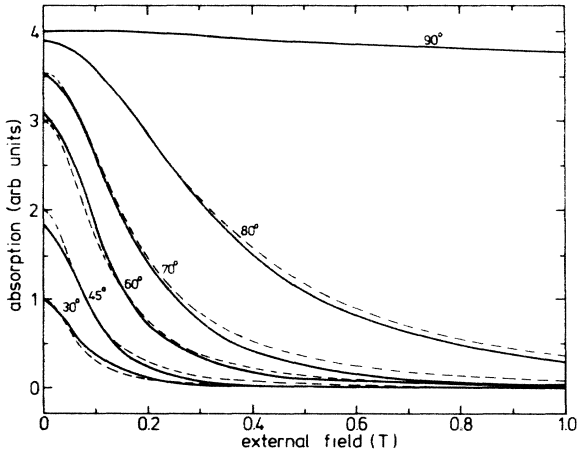

FIG. 7. Microwave spectra of $RbCoCl_3 \cdot 2H_2O$ taken at 9.5 GHz and 4.2 K (solid lines). Angles between static field and c' axis are indicated. Microwave field is perpendicular to static external field. Dashed lines represent the fits according to Eq. (37).

In Fig. 7 we present the microwave absorption at $T = 4.2$ K in the a-c plane when rotating the crystal around the b axis. At a first glance, there are three remarkable features: (1) the maximum absorption occurs at zero external field, (2) there is an orientation where the absorption is independent of the external field, and (3) no absorption was detected perpendicular to that orientation. Careful alignment of the crystal showed that if no absorption was detected, the microwave field is applied perpendicular to the c' axis. Consequently, the external field is directed parallel to c'. On the other hand, rotating the crystal from this position through 90° yields the strongest absorption which turns out to be field independent.

The absorption at zero field y_m, i.e., the top of the absorption curve, is depicted in Fig. 8 as a function of the

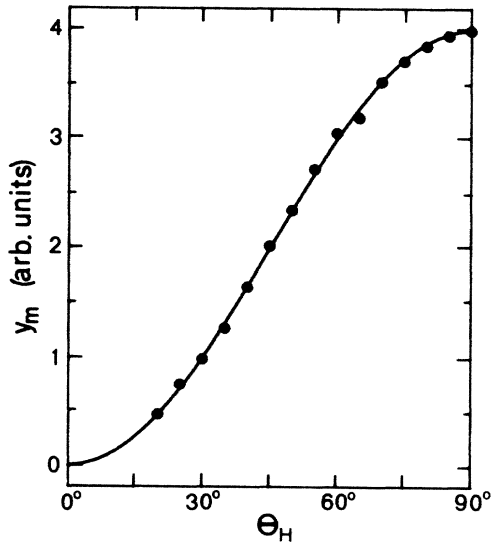

FIG. 8. Angular dependence of microwave absorption in zero field at 4.2 K (solid circles). The solid line represents the fit according to Eq. (35).

angle θ_H between the external field and the c' axis. As the static field is zero, the angular dependence is obviously due to the amount of microwave energy absorbed. By assuming that only the component of the microwave field parallel to c' results in absorption, y_m should obey

$$y_m(\theta_{rf})=y_m^0 \cos^2\theta_{rf} , \tag{35}$$

where θ_{rf} denotes the angle between the direction of the microwave field and the c' axis (in the experiments described, $\theta_{rf}=\theta_H+\pi/2$), and y_m^0 is the absorption if H_{rf} is parallel to c'. The solid curve in Fig. 8 represents Eq. (35) and fits the experimental data very well.

The linewidth Γ as a function of θ_H is given in Fig. 9, where Γ is defined as the field at which the absorption is decreased to half of its maximum value. The solid curve represents

$$\Gamma(\theta_H)=\Gamma_0/\cos\theta_H , \tag{36}$$

where Γ_0 denotes the linewidth if H_c is parallel to c'. These angular dependences, emphasizing the importance of a single direction, establish the metamagnetic character of RCC.[1] Combining Eqs. (35) and (36), we obtain

$$y=y_m^0 \cos^2(\theta_{rf}) f(H\cos\theta_H) , \tag{37}$$

with $f(x)$ the line-shape function. A reasonable fit to all the curves is achieved if $f(x)$ is taken to be Lorentzian,

$$f(x)=1/(1+x^2/\Gamma_0^2) , \tag{38}$$

as shown by the dashed curves in Fig. 7. Therefore, apart from the position of the peak below T_N, the absorption can be simply described by two parameters y_m^0 and Γ_0, both of which turn out to be functions of temperature.

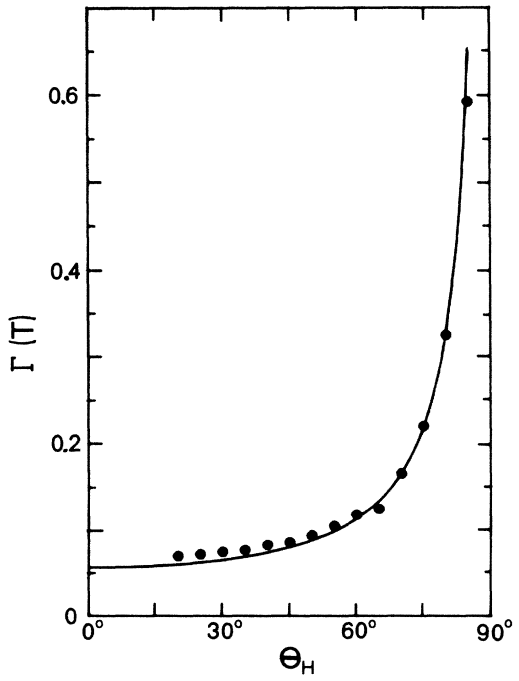

FIG. 9. Angular dependence of linewidth (half-width of half maximum) at 4.2 K (solid circles). The solid line represents the fit according to Eq. (36).

The validity of Eq. (37) was checked in a supporting experiment, which was performed in a second spectrometer, that allowed for varying θ_H independently of θ_{rf}. The angular dependence was confirmed, and as expected from Eq. (37) the best results were obtained for $\theta_H=\theta_{rf}=0$, i.e., both fields parallel along the c' axis. All the measurements described below were obtained in this parallel configuration in the superconducting 3-T equipment.

Spectra were recorded at temperatures between 2.6 and 6.5 K. Outside this interval the signal intensity was too weak to be measured accurately. Three quantities were determined from these spectra: the resonance field, the maximum intensity, and the linewidth.

Above a temperature T_c the top of the resonance curve is observed at zero external field. For temperatures below T_c the field of maximum absorption H_m becomes temperature dependent, as is indicated by the open circles in Fig. 10. The value of T_c is 2.93 ± 0.01 K, which is significantly lower than the Néel temperature ($T_N=2.97\pm0.01$ K). As a good approximation, the line shapes can be considered Lorentzian (cf. Fig. 7), i.e., they follow

$$y=\left[1+\left[\frac{H-H_0}{\Gamma}\right]^2\right]^{-1} , \tag{39}$$

where H_0 is the resonance field and Γ the linewidth. However, in the present case H_0 is very close to zero, and for a detailed analysis the mirror resonance, at negative field, must be taken into account. The actual resonance fields H_0 (indicated by the solid circles in Fig. 10) are evaluated from the observed maxima (open circles). In the same figure we have drawn the magnetic phase boundary between the antiferromagnetic and metamagnetic state (solid curve) as measured by dynamic susceptibility.[14,15] Given the experimental errors, we can conclude that the microwave resonance field coincides with the metamagnetic phase boundary. The phase transition as given in Fig. 10 actually indicates the field of maximum susceptibility, a quantity which strongly depends on the demagnetizating factor.[15] In order to check whether the

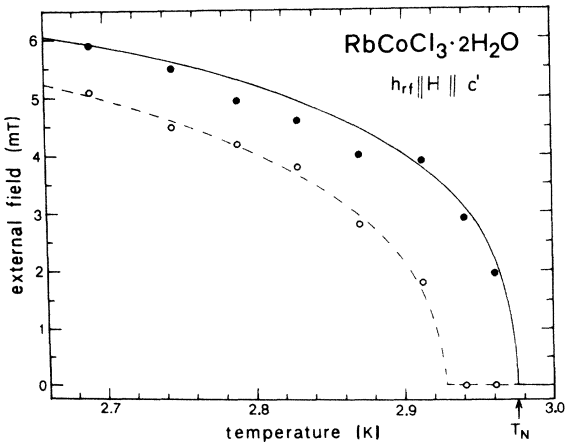

FIG. 10. Resonance field as a function of temperature in parallel-field configuration uncorrected (open circles) and corrected (solid circles) for mirror resonance. The solid curve denotes the metamagnetic phase transition, and the dashed curve is a guide to the eye.

same holds for the resonance field, additional ESR measurements were performed on a sphere-shaped crystal in which we did observe a resonance field at a significantly higher external field. Comparison with dynamic susceptibility experiments on a sphere-shaped crystal[29] results in the conclusion that the resonance actually occurs in the upper region of the mixed phase close to the transition to the induced ferromagnetic state. The maximum of the absorption is observed at zero field for temperatures above T_c. Whether H_0 actually differs from zero is difficult to say. However, at least the upper limit of H_0 can be calculated, and yields $H_0 \leqq 3.7$ mT. Additional measurements at 18 GHz (Ref. 30) showed that, within experimental accuracy, the top of the resonance curve is still located at zero external field. In this case the resonance field is, at least for $\nu < 18$ GHz, (almost) independent of the frequency. A similar observation is made in the case of $CsCoCl_3 \cdot 2H_2O$ (Ref. 8).

The temperature dependence of the maximum absorption y_m at H_m is given in Fig. 11. With decreasing temperature, y_m increases slowly up to a maximum value at about $T = 3.15$ K, after which it decreases very rapidly to almost zero in a region of about 0.5 K. For $T < T_N$, the maximum intensity is corrected for the mirror resonance. The linewidth Γ is found to increase strongly at temperatures $T > T_N$ (Fig. 12). Below T_N the observed linewidth must also be corrected for the mirror resonance and is depicted in the inset of the figure.

B. Magnon-bound states

A straightforward interpretation of the microwave absorption is complicated by the fact that although the spin Hamiltonian has a more or less XY character, the angular behavior, in particular, is more Ising-like. Moreover, there is a great similarity with the ESR results in $CsCoCl_3 \cdot 2H_2O$, which might be regarded as a ZXX antiferromagnet.[8] Furthermore, the relevant temperature region is around the 3D phase transition, thereby excluding the well-known paramagnetic or antiferromagnetic resonances. Therefore, it is tempting to describe the absorption in terms of thermally excited magnon-bound states, as discussed by Torrance and Tinkham for ferromagnetic

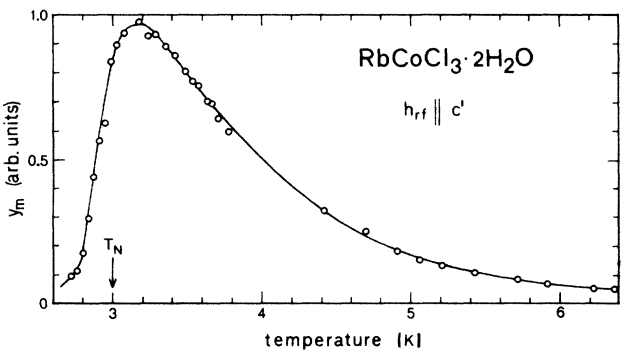

FIG. 11. Maximum of microwave absorption as a function of temperature in parallel-field configuration. Above T_N the maximum is the zero-field value. The solid line is a guide to the eye.

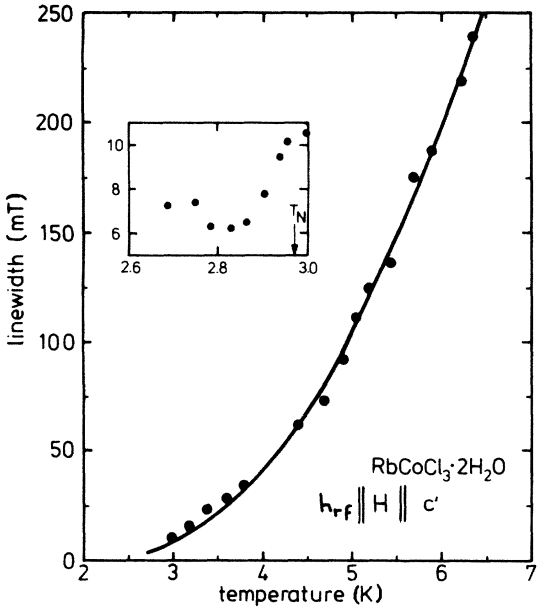

FIG. 12. Linewidth (half-width at half maximum) as a function of temperature. The solid line is a guide to the eye. The inset shows linewidth below T_N, which is corrected for mirror resonance.

ZXX chains,[31] and by Ishimura and Shiba for antiferromagnets.[32]

The model Hamiltonian which serves as a starting point for our discussion slightly deviates from Eq. (29), and reads

$$\mathcal{H}_0 = -2J_0 \sum_l [p(s_l^x s_{l+1}^x + s_l^y s_{l+1}^y) + s_l^z s_{l+1}^z] - h_i \sum_l (-1)^l s_l^z + \mathcal{H}_Z \,, \tag{40}$$

where $p = 0.56$,

$$h_i = g^{zz}\mu_B H_i = g^{zz}\mu_B (H_{e,1}^z + H_d^z)$$

and $\mathcal{H}_Z$ denotes the Zeeman Hamiltonian. Hamiltonian $\mathcal{H}_0$ gives rise to n-magnon–bound states (n-MBS's). The n-MBS is the continuous counterpart of the n-fold spin cluster in Ising systems ($\epsilon = 0$), and evolves towards a state with n decoupled spin waves (or magnons) for a Heisenberg chain ($\epsilon = 1$). The energies of these MBS's are most conveniently evaluated by starting from Ising basis functions[31] and introducing the x and y terms as perturbations.

According to Ishimura and Shiba,[32] we define the Ising basis functions of odd magnon-bound states by

$$\Psi_1(k) = \left[\frac{2}{N}\right]^{1/2} \sum_j e^{ikR_j} s_j^{\pm} \Psi_{\text{Néel},1} \,,$$

$$\Psi_3(k) = \left[\frac{2}{N}\right]^{1/2} \sum_j e^{ikR_j} s_j^{\pm} s_{j+1}^{\mp} s_{j+2}^{\pm} \Psi_{\text{Néel},1} \,, \tag{41}$$

$$\cdots \,,$$

$$\Psi_{n-1}(k) = \left[\frac{2}{N}\right]^{1/2} \sum_j e^{ikR_j} s_j^{\pm} \prod_{\nu=1}^{n/2-1} (s_{j+2\nu-1}^{\mp} s_{j+2\nu}^{\pm}) \Psi_{\text{Néel},1} \,,$$

and, similarly, of the even MBS's by

$$\Psi_2(k)=\left[\frac{2}{N}\right]^{1/2}\sum_j e^{ikR_j}s_j^- s_{j+1}^+\Psi_{\text{Néel},1}\ ,$$

$$\cdots\ , \tag{42}$$

$$\Psi_n(k)=\left[\frac{2}{N}\right]^{1/2}\sum_j e^{ikR_j}\prod_{\nu=0}^{n/2-1}(s_{j+2\nu}^- s_{j+2\nu+1}^+)\Psi_{\text{Néel},1}\ .$$

Here, $\Psi_{\text{Neel},1}$ is one of the two Néel ground states, $s^{\pm}$ denotes the raising and lowering operators, N is the total number of spins, and the angular wave number of k runs over the first Brillouin zone, $-\pi/a<k\leqq\pi/a$. The ordinary spin wave is, of course, $\Psi_1(k)$. We would like to mention here that the magnon-bound states can also be regarded as domain-wall (or soliton) pairs, moving through the chain with the center-of-mass wave vector k.[32] Denoting the total spin by

$$s^z=\sum_i s_i^z\ ,$$

the odd-number MBS's have eigenvalues $s^z=\pm1$, and the even-number MBS's have $s^z=0$.

The matrix elements of $\mathscr{H}_0$ between the functions Ψ_n are now evaluated up to order ϵ.[32,33] If n is odd, we find

$$\langle\Psi_{2\nu-1}\,|\,\mathscr{H}_0\,|\,\Psi_{2\nu'-1}\rangle=\begin{cases}2[\,|J_0|+(2\nu-1)h_i], & \nu'=\nu\\ V, & \nu'=\nu+1\\ V^*, & \nu'=\nu-1\\ 0, & \text{otherwise}\ ,\end{cases} \tag{43}$$

where $V=p\,|J_0|(1+e^{-2ika})$, with a the interatomic distance in the chain, while zero external field is assumed. In the case of even MBS's the diagonal elements read $2(|J_0|+2\nu h_i)$. If $h_i=0$ and $p\ll1$, the energies, calculated relative to the energy of the ground state $\Psi_{\text{Neel},1}$, are obtained in a straightforward way, yielding[32]

$$E=2\,|J_0|\,[1-2p\cos(ka)\cos(ka+\phi)]\ , \tag{44}$$

with $-\pi<\phi\leqq\pi$. They form a continuous band around $E=2\,|J_0|$; for $p=0$ (true Ising) all states are degenerated at $2\,|J_0|$. Johnson *et al.*[34] have given a (complicated) expression for arbitrary p, which yields the correct gapless dispersion relation for $p\to1$. Shiba[33] numerically evaluated the energies for $h_i\neq0$ and $p\ll1$. An analytical solution for this case is obtained by mapping the Hamiltonian, Eq. (40), onto a ferromagnetic Hamiltonian.[35] In the latter case the solutions are given in terms of Bessel functions,[36] and the energies for the even states at the lower-band edge ($\phi=-\pi$) read

$$E_\kappa^{\text{even}}=2\,|J_0|\,(1-2\,|p\cos(ka)|\,\{1-\tfrac{1}{2}[3\pi(\kappa+\tfrac{3}{4})h_i/2\,|pJ_0\cos(ka)|\,]^{2/3}\})\ , \tag{45}$$

with $\kappa=0,1,2,\ldots$. Energies for the odd MBS's are given by $E_\kappa^{\text{odd}}=E_\kappa^{\text{even}}-h_i$. From Eq. (45) it is seen that the energies in the continuum are quantized on introducing a staggered field h_i. Note that a nonstaggered field in the z direction only shifts the energies of the continuum. When applying an external magnetic field, staggered components in the z direction are generated by fields in the x-y plane [cf. Eq. (33)], which can be considered additive to h_i.

The energies for the $k=0$ modes, relevant to the ESR problem, cannot be retrieved from Eqs. (44) and (45) for arbitrary values of p. To obtain an estimate for the gap energy we have calculated the dispersion relation in the spin-wave approximation. For the sake of completeness we started from the original Hamiltonian [Eq. (29), including unequal weight factors p and q for s^x and s^y, respectively], and took into account a staggered field h_i in the z direction. The result, up to first order in the Holstein-Primakoff transformation, yields

$$(E_\pm)^2=[2\,|J_0|\pm|J_0|\,(p-q)\cos(ka)+h_i]^2-|J_0|^2(p+q)^2\cos^2(ka)\ , \tag{46}$$

where the value $s=\frac{1}{2}$ is substituted. In the limit $p=q=1$ and $h_i=0$, the correct dispersion for an antiferromagnetic Heisenberg chain is found. The result for $p=q\ll1$ differs from Eq. (44), the origin of which must be found in the different way of performing the perturbation.

C. Discussion

Before going into the details of the ESR results, we shall first reconsider the Zeeman Hamiltonian, as specified formally in Eqs. (32) and (33). From the latter the preferred direction of $\chi^{a\text{-}c}$ (and the magnetic moment $\mu^{a\text{-}c}$ at high temperatures) was found to be the c'' axis (Fig. 6). A transformation of the tensor $\underline{G}_l$ [Eq. (33)] around z to a set of axes, c'' and $c_\perp''$, for the Zeeman Hamiltonian, yields

$$\mathscr{H}_Z=\mu_B\sum_l|g^{x'x'}s_l^{x'}H^{x'}+g^{y'y'}s_l^{y'}H^{y'}+g^{zz}s_l^zH^z+(-1)^lg^{x'y'}(s_l^{x'}H^{y'}+s_l^{y'}H^{x'})+(-1)^lg^{y'z}(s_l^{y'}H^z+s_l^zH^{y'})|\ , \tag{47}$$

with

$$g^{x'x'}=3.2,\ \ g^{y'y'}=4.4\ ,$$
$$g^{x'y'}=0.5,\ \ g^{y'z}=1.6\ . \tag{48}$$

The last term gives a staggered field in the z direction, and is therefore simply additive to the internal staggered field in Eq. (40). Note that a field applied in the x' direction does not give a z component. As has been discussed at the end of Sec. IV, for low temperatures the c' axis is the important direction, and not the c''. Thus from now on we take, on phenomenological grounds, the c' axis to

be the y' direction in Eq. (47).

As to the nature of the microwave absorption, we make an estimate for the $k=0$ energy from Eq. (46), yielding $E_-(k=0)=9.4$ K. This energy is far beyond our experimental range, and makes the possibility of creating the elementary excitations very unlikely. The origin of the ESR absorption must therefore be found in making transitions between thermally created excitations, of which the magnon-bound state is considered to be the best candidate.

The frequency-field relations of the MBS resonances are readily obtained from Eq. (45). It is noted in between that the transformation discussed above also affects the exchange Hamiltonian in that weak off-diagonal (symmetric) $x'y'$ terms will appear. As our discussion is, however, semiquantitative, we shall not consider this point further. Two types of transitions are possible: (i) a $\Delta s^z=\pm 1$ transition between an even- and an odd-numbered MBS, and (ii) a $\Delta s^z=0$ transition between two even- or two odd-numbered MBS's. If we now apply the microwave field along the c' (or y') axis, it can be seen from Eq. (47) that a Zeeman contribution is present in the y' as well as in the z direction. Therefore the selection rules allow for both types of transitions. For the resonance condition of the $|\Delta s^z|=1$ transitions induced by the rf Zeeman term in the y' direction, we obtain

$$\hbar\omega = E^{\text{even}} - E^{\text{odd}} = g^{y'z}\mu_B H_{\text{eff}} , \tag{49}$$

where we introduced the effective field

$$H_{\text{eff}} = (g^{zz}/g^{y'z})H_i + H_0 ,$$

and H_0 in the c' direction. It is obvious from Eq. (49) that if X-band absorption is observed around zero external field ($H_0 \simeq 0$), absorption at nonzero field should be detected at double the frequency. The fact that this has not been observed makes the $|\Delta s^z|=1$ transition highly unlikely.

As to the $\Delta s^z=0$ resonances, we infer from Eq. (45) that, for $k=0$,

$$\hbar\omega = E_{\kappa+1} - E_\kappa = 2p\,|J_0|\,(3\pi g^{y'z}\mu_B H_{\text{eff}}/2p\,|J_0|)^{2/3} \times [(\kappa+\tfrac{7}{4})^{2/3} - (\kappa+\tfrac{3}{4})^{2/3}] . \tag{50}$$

This relation is depicted in Fig. 13 for $\kappa=0$, 1, and 2. Included are the two experimental points, where we have drawn the $\kappa=0$ curve through the 9.5-GHz point. Thus the almost frequency-independent resonance field can be satisfactorily explained by assuming that $\Delta s^z=0$ MBS resonances are observed. Using $\omega=19\pi$ GHz and $\kappa=0$, we derive from Eq. (50) an effective field of $H_{\text{eff}}=150$ Oe. At 4.2 K, $H_0=0$ and thus H_{eff} is an estimate for the internal field above T_N. Below T_N the resonance field shifts from zero (Fig. 10) and coincides with the metamagnetic transition. This field in the c' direction must be considered a compensation of the internal field. The angular behavior of the microwave absorption, being a manifestation of strong anisotropy, is now easily understood from the form of the Zeeman Hamiltonian. A $\Delta s^z=0$ transition requires a Zeeman component in the z direction. When applying the rf field in the a-c plane, this is only accomplished by the component in the y' (or c') direction. The angular dependence of the dc field is explained in a similar way. Only the staggered Zeeman component along s_i^z influences the splitting of the MBS's and, hence, the observed absorptions. This component is induced by a dc field parallel to the c' axis only. A nonstaggered external field in the z or even in another direction shifts the absolute energy levels an equal amount for all κ,[37] and, consequently, disappears from the resonance condition (50).

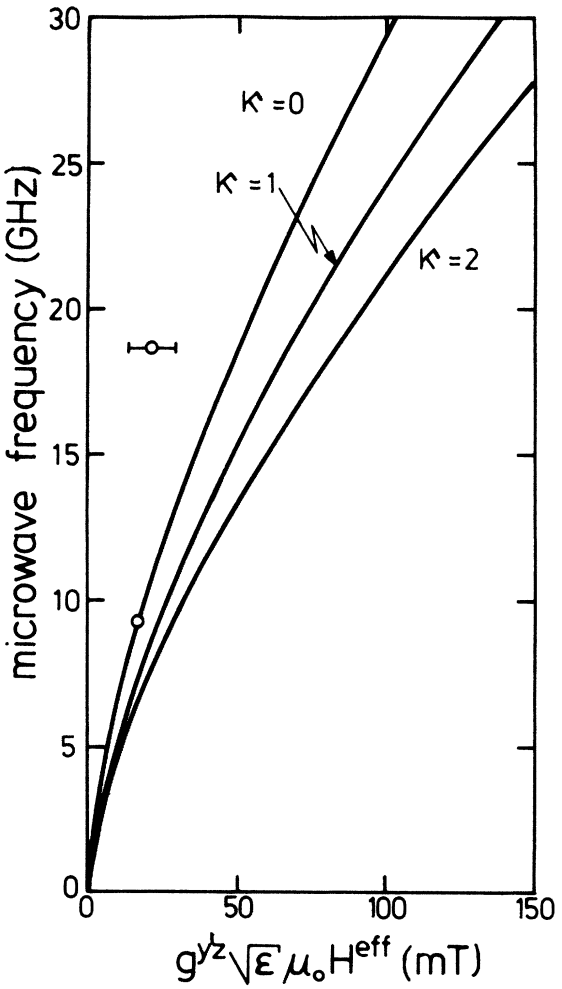

FIG. 13. Magnon-bound state resonances for $\kappa=0$, 1, and 2, according to Eq. (50), as a function of effective field. Open circles denote data points at 9.5 and 18 GHz.

We now turn to the intensity of the absorption as a function of temperature. The ESR intensity, defined as the area under the absorption curve, is plotted versus temperature in Fig. 14. It is noted, in the first place, that the overall temperature behavior is characteristic for resonance between thermally activated excitations in a linear chain, a process which is quite well understood in Ising-like systems.[38] The intensity increases from zero with increasing temperatures due to the thermal activation of more MBS's. Above a maximum the intensity gradually decreases to zero as a consequence of decreasing correlation length and interactions between MBS's in different chains. An expression for the intensity as a function of temperature is only available for $\epsilon \ll 1$,[39] but is difficult

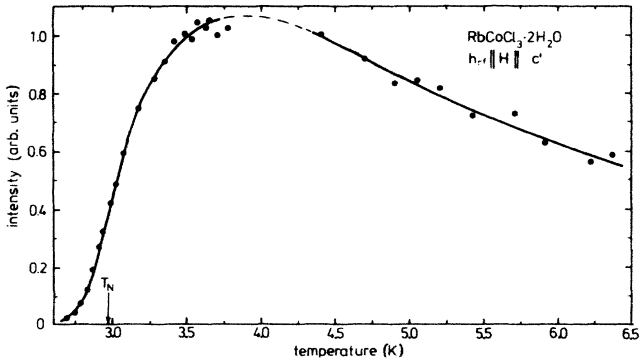

FIG. 14. Intensity of microwave absorption (area under spectral line) as a function of temperature. The solid line is a guide to the eye.

to deal with. Therefore we restrict ourselves, as a first approximation, to the Ising theory.[38,40] Just above T_N, an exponential behavior (Fig. 15) is found according to

$$I \sim \exp(-E/k_B T) , \tag{51}$$

with $E/k_B = 26 \pm 2$ K, as is represented by the solid line. This energy equals $2J_0$ in the Ising limit, yielding $J_0/k_B = 13$ K, a value which is very close to the exchange constant previously presented. Below T_N even the true spin-cluster model is unable to explain the dramatic decrease of intensity. What happens is that in that temperature region the internal (staggered) field rises very rapidly.

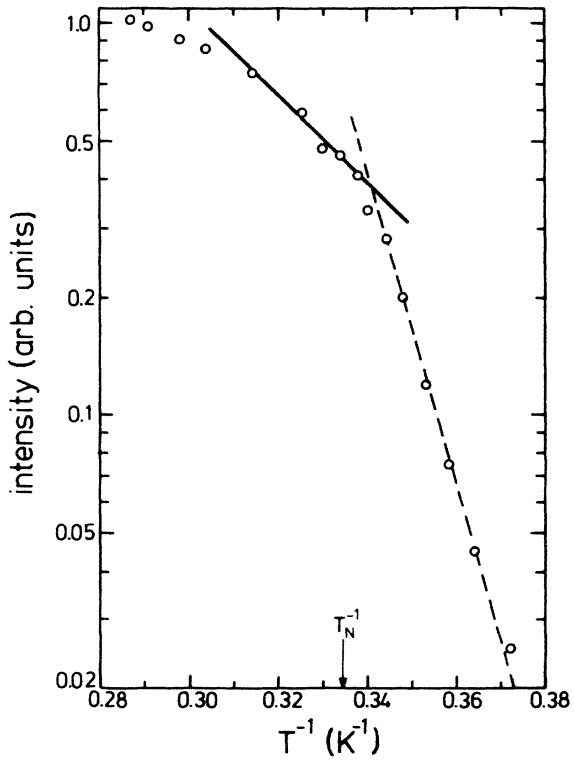

FIG. 15. Magnon-bound state resonance intensity versus reciprocal temperature. The fits are according to Eq. (51) for $E/k_B = 26$ K (solid line) and $E/k_B = 93$ K (dashed line).

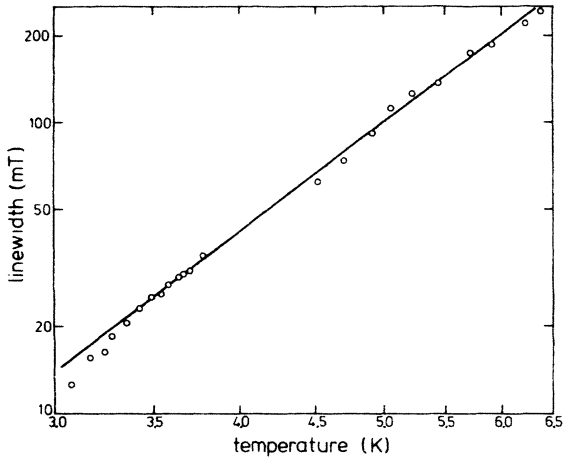

FIG. 16. Linewidth versus temperature on double-logarithmic scale. The solid line is $\Gamma \sim T^{\alpha}$, with $\alpha = 3.9$.

This can also be seen from the sublattice magnetization, which rises to 90% of its maximum value at $T = 0$ between T_N and 2.6 K.[15] This happens to be just the interval where the intensity disappears. As is clear from Fig. 13, a large staggered field will take the resonance out of the experimental region.

Finally, we look more closely at the linewidth. In order to obtain better insight, we have plotted Γ as a function of temperature on a double-logarithmic scale (Fig. 16). We find that, for $T > T_N$,

$$\Gamma \sim T^{3.9} . \tag{52}$$

To the best of our knowledge, an expression for the temperature dependence of the linewidth of spin-cluster or MBS resonance is not available. The linewidth of the antiferromagnetic resonance ($\epsilon = 1$), however, has been studied by several authors.[41,42] The calculations of Rezende and White based on a theory of multimagnon processes in the ordered state yield a temperature dependence of

$$\Gamma \sim T^{\alpha} , \tag{53}$$

where $\alpha = 2$ or 4, depending on the dimensionality and temperature region. Although the observed T^4 behavior is encouraging, we must interpret it with care. Firstly, we cannot account for the order of magnitude of the linewidth, and secondly the present compound is not of true Heisenberg type. On the other hand, the resemblance of the dynamics to a case intermediate between magnons and MBS's is clear. The uniform modes of the bound states (i.e., $k = 0$), as excited by microwaves, decay due to interactions with modes having $k \neq 0$.

In conclusion, it can be said that the MBS resonances give a good explanation for the frequency behavior as well as for the angular dependence of the ESR spectra in $RbCoCl_3 \cdot 2H_2O$. When absolute energies do play a significant role, as is the case when considering intensities, the model is too much of a simplification. It should then be extended for a larger ϵ, and the dipolar and interchain exchange energies must be taken into account more accurately.

VI. SUMMARY AND CONCLUSIONS

In this paper we have reconsidered the spin Hamiltonian of $RbCoCl_3 \cdot 2H_2O$ on the basis of a detailed crystal-field analysis. Although the canting of the $Cl_4(H_2O)_2$ octahedra that surround the Co ions is not exclusive for RCC, it has far-reaching consequences in the present compound. The fact that the principal axes of the two types of octahedra are almost perpendicular to each other leads to a spin Hamiltonian of more or less XY character. Experimental information, needed for details on the crystal-field parameters and g factors, was extracted from high-temperature susceptibilities. In addition, the intrachain exchange constant was obtained, yielding $J_0/k_B = -14.6$ K. This value is in agreement with results from low-temperature susceptibilities. By use of the calculated g tensor, the magnitude and direction of the magnetic moment in the ordered state, as measured by neutron diffraction, could be confirmed. As the theory included a high-temperature approximation, and did not incorporate 3D interactions, the precise direction of the c' axis was, however, not predicted. The results of the present analysis also allow a detailed insight into the various contributions to susceptibility and magnetization at low temperatures. Canting of the moments can be satisfactorily explained from the canted crystallographic structure in combination with single-ion anisotropy, and the introduction of an antisymmetric exchange seems superfluous.

The nature of the elementary excitations in RCC was probed by ESR. Microwave absorption was found around the 3D phase transition. It showed strong angular dependence relative to the c' axis, and hardly any frequency dependence. The results are best explained in terms of thermally excited magnon-bound states, which are considered to be the elementary excitations of the anisotropic Heisenberg Hamiltonian. Because of the strong resemblance to the antiferromagnetic resonance results in $CsCoCl_3 \cdot 2H_2O$, a reconsideration of the latter data in terms of magnon-bound states would be worthwhile.

ACKNOWLEDGMENTS

We thank C. H. W. Swüste from Eindhoven University of Technology for making available unpublished experimental results at 18 and 28 GHz, and J. Flokstra for unpublished susceptibility measurements and stimulating discussions.

APPENDIX

The transformation from the crystallographic axes x'',y'',z'' to the local axes ξ,η,ζ is accomplished by three successive rotations over the angles ϕ, θ, and ψ (cf. Fig. 2). A vector $\mathbf{X}''$ in the former system is then related to Ξ in the local system according to

$$\Xi = \underline{R}_1 \mathbf{X}'' , \tag{A1}$$

where

$$\underline{R}_1 = \begin{bmatrix} \cos\psi\cos\phi - \sin\psi\sin\phi\cos\theta & \cos\psi\sin\phi + \sin\psi\cos\phi\cos\theta & \sin\psi\sin\theta \\ -\sin\psi\cos\phi - \cos\psi\sin\phi\cos\theta & -\sin\psi\sin\phi + \cos\psi\cos\phi\cos\theta & \cos\psi\sin\phi \\ \sin\phi\sin\theta & -\cos\phi\sin\theta & \cos\theta \end{bmatrix} \tag{A2}$$

for ion (1). In case of ion (2), $\phi \rightarrow \phi + \pi$; hence, $\underline{R}_2(\phi) = \underline{R}_1(-\phi)$. Furthermore, $\underline{R}_j^{-1} = \underline{R}_j^T$, with $j = (1,2)$, and $\underline{R}^T$ denotes the transposed matrix.

Expressing the exchange interaction [Eq. (7)] on the local axes is accomplished by

$$\mathscr{H}_e = -2J\mathbf{S}_1^T \underline{I} \mathbf{S}_2 = -2J\boldsymbol{\Sigma}_1^T \underline{E} \boldsymbol{\Sigma}_2 , \tag{A3}$$

where $\boldsymbol{\Sigma}_1, \boldsymbol{\Sigma}_2$ are the spins in local-axes notation, $\underline{I}$ the unit matrix, and $\underline{E}$ the matrix

$$\underline{E} = \begin{bmatrix} \alpha & \nu & \rho \\ \nu & \beta & \sigma \\ \rho & \sigma & \gamma \end{bmatrix} , \tag{A4}$$

with

$$\begin{aligned} \alpha &= -[\cos^2\psi + \cos(2\theta)\sin^2\psi] , \\ \beta &= -[\sin^2\psi + \cos(2\theta)\cos^2\psi] \\ \gamma &= \cos(2\theta) , \\ \nu &= \tfrac{1}{2}[1 - \cos(2\theta)]\sin 2\psi , \\ \rho &= \sin(2\theta)\sin\psi , \\ \sigma &= \sin(2\theta)\cos\psi . \end{aligned} \tag{A5}$$

The $\boldsymbol{\Sigma}$ notation for the spins in (A3) is only formal. Throughout this paper we have denoted the spins by $\mathbf{S}$ ($\mathbf{s}$), while the interpretation will be clear from the context.

*Permanent address: Departamento de Física, Escuela Técnica Superior de Ingenieros Industriales, Universidad de Zaragoza, Zaragoza, Spain.

[1] E. Stryjewski and N. Giordano, Adv. Phys. **26**, 487 (1977).
[2] J. A. J. Basten, Q. A. G. van Vlimmeren, and W. J. M. de Jonge, Phys. Rev. B **18**, 2179 (1978).
[3] A. L. M. Bongaarts and B. van Laar, Phys. Rev. B **6**, 2669 (1972).
[4] R. D. Spence and A. C. Botterman, Phys. Rev. B **9**, 2993 (1974).
[5] A. J. W. A. Vermeulen, E. Frikkee, J. Flokstra, and W. J. M. de Jonge, Physica **98B**, 205 (1980).
[6] Q. A. G. van Vlimmeren and W. J. M. de Jonge, Phys. Rev. B **9**, 1503 (1979).

[7]H. Th. LeFever, R. C. Thiel, W. J. Huiskamp, and W. J. M. de Jonge, Physica **111B**, 190 (1981).
[8]A. Herweijer, W. J. M. de Jonge, A. C. Botterman, A. L. M. Bongaarts, and J. A. Cowen, Phys. Rev. B **5**, 4618 (1972).
[9]A. L. M. Bongaarts and W. J. M. de Jonge, Physica **86-88B**, 595 (1977).
[10]D. B. Losee *et al.*, Phys. Rev. B **8**, 2185 (1973).
[11]Y. Okuda, H. Nishikawa, and M. Matsuura, J. Phys. Soc. Jpn. **50**, 31 (1981).
[12]J. N. McElearney and S. Merchant, Phys. Rev. B **18**, 3612 (1978).
[13]S. Harkema and W. van der Graaf, Inorg. Nucl. Chem. Lett. **11**, 813 (1975).
[14]J. Flokstra, G. J. Gerritsma, B. van den Brandt, and L. C. van der Marel, Phys. Lett. **53A**, 159 (1975).
[15]J. Flokstra, G. J. Gerritsma, A. J. W. A. Vermeulen, E. Frikkee, and W. J. M. de Jonge (unpublished).
[16]E. J. Nijhof, H. van der Vlist, J. A. Puértolas, and G. J. Gerritsma, in *Proceedings of the XXIInd Congress Ampère,* edited by K. A. Müller, R. Kind, and J. Roos (The University of Zürich, Zurich, 1984), p. 141.
[17]The angle of 22° is now well established from susceptibility and ESR measurements. The value of 28°, as given in Refs. 12 and 14, must be considered doubtful.
[18]J. A. Rojo, J. Bartolome, G. Navarro, D. Gonzalez, and A. J. Van Duynevelt, in Proceedings of XVIII Real Sociedad Española de Física y Química 11.17 G (1980) (unpublished).
[19]H. J. M. ter Brake, J. A. Ulfman, and J. Flokstra, J. Phys. E **17**, 1024 (1984).
[20]T. Oguchi, J. Phys. Soc. Jpn. **20**, 2236 (1965).
[21]A. Narath, Phys. Rev. **140**, A552 (1965).
[22]M. E. Lines, Phys. Rev. **131**, 546 (1963).
[23]I. F. Silvera, J. H. M. Thornley, and M. Tinkham, Phys. Rev. **136**, A695 (1964).
[24]Q. A. G. van Vlimmeren, Ph.D. thesis, Eindhoven University of Technology, Eindhoven, 1979 (unpublished).
[25]H. A. Groenendijk and A. J. van Duyneveldt, Physica **115B**, 41 (1982).
[26]A. Abragam and B. Bleaney, *Electron Paramagnetic Resonance of Transition Ions* (Clarendon, Oxford, 1970).
[27]E. J. Nijhof, Ph.D. thesis, Twente University of Technology, Enschede, 1985 (unpublished).
[28]T. Moriya, Phys. Rev. **120**, 91 (1960).
[29]M. Chirwa, Ph.D. thesis, Twente University of Technology, Enschede, 1985 (unpublished).
[30]C. H. W. Swüste (unpublished results).
[31]J. B. Torrance and M. Tinkham, Phys. Rev. **187**, 587 (1969).
[32]N. Ishimura and H. Shiba, Prog. Theor. Phys. **63**, 743 (1980).
[33]H. Shiba, Prog. Theor. Phys. **64**, 466 (1980).
[34]J. D. Johnson, S. Krinsky, and B. M. McCoy, Phys. Rev. A **8**, 2526 (1973).
[35]I. Bose and S. Chatterjee, J. Phys. C **16**, 6681 (1983).
[36]H. C. Fogedby and H. H. Jensen, Phys. Rev. B **6**, 3444 (1972).
[37]K. Adachi, J. Phys. Soc. Jpn. **50**, 3904 (1981).
[38]E. J. Nijhof, G. J. Gerritsma, and J. Flokstra, Physica **122B**, 333 (1983).
[39]H. Yoshida and T. Ishikawa, J. Phys. Soc. Jpn. **50**, 1119 (1981).
[40]G. D. Berim, M. M. Zaripov, and A. R. Kessel, Zh. Eksp. Teor. Fiz. **66**, 734 (1974) [Sov. Phys.—JETP **39**, 355 (1974)].
[41]S. M. Rezende and R. M. White, Phys. Rev. B **14**, 2939 (1976).
[42]A. B. Harris, J. Appl. Phys. **37**, 1128 (1966).